CHEMICAL PHYSICS

K. Yamanouchi
A. Becker
R. Li
S. L. Chin (Eds.)

# Progress in Ultrafast Intense Laser Science IV

Springer
PUILS
JILS

Kaoru Yamanouchi
Andreas Becker
Ruxin Li
See Leang Chin
(Eds.)

# Progress in Ultrafast Intense Laser Science

## Volume IV

With 133 Figures

Springer

# Contents

# 8

# Ultrashort Pulse Collapse in Quadratic Media

Jian Wu and Heping Zeng

**Abstract.** Experimental studies on spatiotemporal collapse of ultrashort pulse propagation in quadratic nonlinear media are reviewed. Two-dimensional multicolored transverse arrays are experimentally observed in a quadratic nonlinear medium based on cascaded non-collinearly quadratic couplings and spatial breakup of input pump beams. Furthermore, two-dimensional multicolored up-converted parametric amplifications are realized with preserved coherence. The observed two-dimensional arrays can be controlled by changing the boundary condition with a weak second harmonic beam along with the strong fundamental-wave pump pulses. As a result of spatiotemporal collapse of femtosecond pulses, colored conical emissions are observed under strong phase-matched fundamental pump, which are further amplified to support tunable broadband femtosecond pulse generation.

## 8.1 Introduction

In the ultrafast high-intensity laser interaction regime, strong optical fields may induce quite a lot of novel phenomena with many unrevealed intrinsic physics even only some basic nonlinear optical processes, such as second harmonic generation and optical parametric amplification, are considered. Recent studies on self-focusing behaviors of intense ultrashort pulses indicated that spatial and temporal degrees of freedom could not be treated separately [1]. Spatiotemporal modulational instability [1, 2] occurs in the presence of both diffraction and dispersion that act together with the material nonlinearities to defeat the spatial spreading and temporal broadening of optical wave-packet, which may induce spatiotemporal collapse of optical wave-packet, such as x-shaped light bullets [1], colored conical emission [2], and spatiotemporal solitary waves. Taking the well-known second harmonic generation process in quadratic nonlinear media as an example, strong mutual interaction and energy exchange between the involved optical fields at different frequencies can bring about some intriguing phenomena for the nonlinear wave propagations. Quadratic spatial solitons are typically observed as quadratic nonlinearities defeat transverse diffractions in quadratic nonlinear

media. Furthermore, multiple quadratic spatial solitons are observed as reproducible one-dimensional spatial patterns in quadratic nonlinear media near phase-matched second harmonic generation by means of spatial modulational instabilities [3], or spontaneous amplification of small input beam asymmetries or material anisotropies [4–8]. All-optical control of one-dimensional quadratic spatial solitons has been realized by either seeding a weak second harmonic (SH) beam or changing the input beam asymmetries [7, 8]. However, pump intensities required for the direct observation of two-dimensional quadratic spatial solitons are usually much higher than the material damage thresholds [3]. Breaking the barriers to produce two-dimensional arrays needs new experimental approaches. From the practical application points of view, quadratic nonlinearities have been extensively applied to the generation of spatial and spatiotemporal solitary waves [1, 3–5], optical switching [9], pulse self-compression [10], mode-locking of femtosecond lasers [11], and so on. The generation of two-dimensional multicolored transverse arrays can help us to explore the fundamental physics of two-dimensional transient gratings and stimulate some applications such as multicolored amplifications, ultrashort pulse generation, and all-optical control such as carrier-envelope-phase control of tunable multicolored coherent optical source. Moreover, multiple three-photon processes could be involved in phase-matched second harmonic generation, and the accompanied spatiotemporal modulational instabilities could cause perturbations with certain frequencies to grow at given geometric angles governed by the phase-matching conditions, leading to colored conical emissions [2]. Such spatiotemporal collapse of ultrashort pulse is much more complicated than the typical case with only the spatial effects involved, and intensive experimental investigations are required to fully understand the dynamics and intrinsic physics of colored conical emissions in quadratic nonlinear media.

In this review article, we present the experimental observation of two-dimensional multicolored transverse arrays under the pump of two crossly overlapped femtosecond (fs) beams in a quadratic nonlinear medium [12]. The formation of two-dimensional arrays is based on the spatial breakup of an input elliptical beam, which interacts with the other pump beam non-collinearly through cascaded non-collinearly quadratic couplings. Two-dimensional transient gratings are formed, which could be probed with either a super-continuum pulse or a weak fundamental-wave (FW) beam, leading to two-dimensional multicolored up-converted parametric amplifications or enhanced two-dimensional multicolored transverse arrays, respectively. Seeding with a weak SH beam, the two-dimensional arrays could be suppressed on the basis of a controllable change of the boundary condition of the induced spatial breakup of the elliptic input beam. We also present the experimental observation of colored conical emissions in a thick quadratic nonlinear medium at a high-intensity pump, which extends the horizon of wave-packet collapse to the spatiotemporal domain [13]. Assisted by the spatiotemporal modulational instabilities, seeded amplification of colored conical emission exhibits a

widely tunable range in wavelength and high energy conversion efficiency [14], which could be further used to generate carrier envelope phase stabilized pulse by nonlinear frequency mixing with the FW pump pulse.

## 8.2 Two-Dimensional Multicolored Transverse Arrays

The experiments reported throughout this article were carried out by using an amplified Ti:Sapphire system consisting of a mode-locked oscillator and a regenerative amplifier. The system generates 50 fs pulses of about 650 μJ per pulse at a 1 kHz repetition rate with central wavelength at 800 nm. The quadratic nonlinear medium used to generate two-dimensional multicolored transverse arrays is a 4 mm thick beta-barium borate (BBO, type I, 29.18° cut). As shown in Fig. 8.1a, the fs pulse from the laser system was split into an on-axis beam $\overrightarrow{k_1}$ and a slightly off-axis beam $\overrightarrow{k_2}$. The $\overrightarrow{k_1}$ beam was focused into the BBO crystal by a high-reflection spherical concave mirror of 2,000 mm curvature radius with a fold angle of 12°. This led to an elliptically spatial profile of $\overrightarrow{k_1}$ beam as $W_y/W_x = 1.58$, where $W_x$ and $W_y$ are the beam widths. While, the $\overrightarrow{k_2}$ beam was round and collimated down to the BBO crystal through a telescope system. At the input facet of the BBO crystal, the beam diameter along the long-axis direction was measured to be about 1.3 mm. The BBO crystal was placed about 200 mm before the focusing position for the sake of avoiding damage and adjusted to fulfill second harmonic generation for the on-axis $\overrightarrow{k_1}$ beam at 800 nm.

As presented in Fig. 8.1b, additional spatial patterns beside the original beam were observed after the BBO crystal as a result of wave-packet breakup of the spatially elliptical on-axis beam $\overrightarrow{k_1}$ with a self-induced spatially varying transverse phase properly balancing the effect of diffraction, where the mutual interactions between the FW and SH pulses played crucial roles [7, 8, 15–17]. The situation changed when a weak SH beam was seeded at the input of the crystal along with the on-axis $\overrightarrow{k_1}$ beam, which modified the induced spatially transverse phases and eventually influenced the wave-packet breakups. In order to demonstrate those effects, as shown in Fig. 8.1b, an additional 1 mm thick BBO crystal (labeled as BBO2) was placed before the original 4 mm BBO crystal (labeled as BBO1) to generate a weak SH beam collinearly with the on-axis FW beam. Here, BBO1 and BBO2 crystals are used for wave breakup observation and control, respectively. The pulse energy ratio SH/FW could be changed by adjusting the phase-matching condition of the 1 mm thick BBO crystal. As presented in Fig. 8.1b, the wave-packet breakup could be suppressed as the pulse energy ratio SH/FW reached 3.6%. Obviously, the generation of multiple one-dimensional quadratic spatial solitons was controllable by seeding along a weak SH beam at the input of the quadratic nonlinear crystal [8]. In order to verify our experimental observations, numerical simulations were carried out

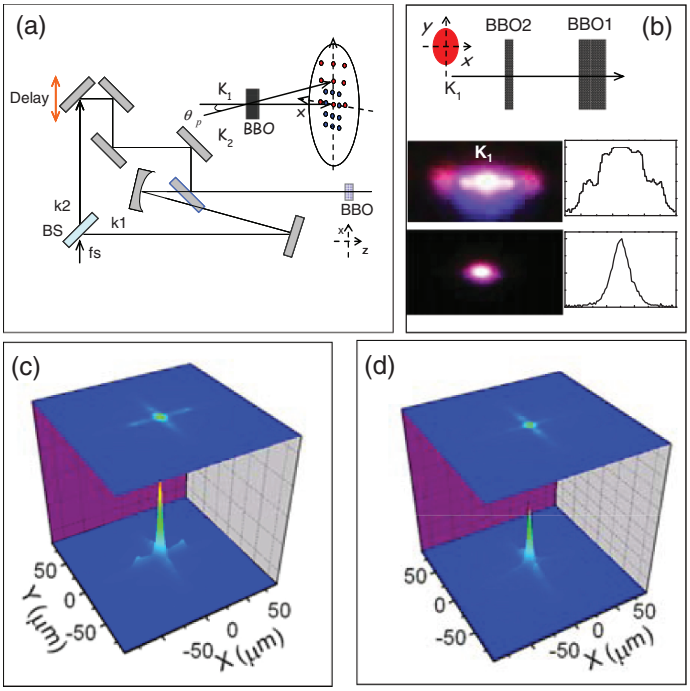


**Fig. 8.1.** (**a**) Schematic for generation of two-dimensional multicolored transverse arrays in a quadratic nonlinear medium. (**b**) Experimental scheme for generation and weak beam control of one-dimensional multiple quadratic spatial solitary waves. Experimentally observed pictures and corresponding transverse intensity spectra are presented as the insets. The wave breakup is suppressed as the pulse energy ratio SH/FW reached 3.6%. The numerical results of the quadratic nonlinearities induced wave breakup of FW pulse with the pulse energy ratios SH/FW as 0 and 3.0% are presented in (**c**) and (**d**), respectively. BS: beam splitter

by solving the $(3+1)$-dimensional nonlinear equations governing the second harmonic generation process in a BBO crystal (type I phase-matching) with a spatially elliptic FW beam as the initial input. As shown in Fig. 8.1c, d, after propagation in a 4 mm thick BBO crystal, quadratic nonlinearities induced a wave-packet breakup of the FW beam with a small input asymmetry, which could be further suppressed as a weak SH beam was initially seeded along the FW beam.

Two-dimensional multicolored transverse arrays were generated as both the on-axis $\overrightarrow{k_1}$ and off-axis $\overrightarrow{k_2}$ beams were synchronized in the 4 mm thick BBO crystal at a crossing angle $\theta_p$ and spatially overlapped each other in a scheme as shown in Fig. 8.1a. New patterns with a frequency shift (determined by the phase-matching condition) was generated based on the cascaded noncollinearly quadratic processes between the novel beams induced by spatial breakup of $\overrightarrow{k_1}$ and the input off-axis beam $\overrightarrow{k_2}$. The generated new multicolored

patterns participated in cascaded non-collinearly quadratic processes in turn and eventually produced two-dimensional periodic patterns. As presented in Fig. 8.2a, reproducible two-dimensional multicolored transverse arrays were directly observed after the BBO crystal with pump intensities much lower than the damage threshold of the nonlinear medium. Overall, there are two sets of well-resolved red and blue arrays. For clarity of description later on, we label those two-dimensional patterns as $R(n, m)$ and $B(n, m)$, starting with $R(0, 0)$ and $B(0, 0)$ that correspond to the FW and SH of $\overrightarrow{k_1}$ beam, respectively. The other patterns are labeled in a reference frame of $(x,\ y)$ with the grid origin $R(0, 0)$ for red patterns (and $B(0, 0)$ for blue patterns), and some examples are presented in Fig. 8.2a. As a result of the required phase-matching in the cascaded non-collinearly quadratic processes, the spectra of the blue and red patterns varied at different rows and columns. The beam divergences of the red and blue patterns were measured, which showed typical values as $\Delta\theta_x \sim 1.2^\circ$ ($\Delta\theta_y \sim 1.8^\circ$) and $\Delta\theta_x \sim 0.7^\circ$ ($\Delta\theta_y \sim 1.1^\circ$), respectively. Two-dimensional multicolored transverse arrays with different conically angular spectra could be observed as the crossing angle $\theta_p$ was changed. Well-resolved red and blue patterns could be observed with enough large $\theta_p$, and denser rows of transverse spots could be observed with smaller $\theta_p$. However, due to the divergences of the transverse spots, the two-dimensional multicolored transverse arrays became blurred in the far-field observation screen for a small $\theta_p$ ($\theta_p \sim 1.26^\circ$). As limited by the typical divergence of the observed two-dimensional patterns, the two-dimensional multicolored transverse arrays exhibited no resolved rows with $\theta_p < 2\Delta\theta_x$. Nevertheless, we note that the angular separation of adjacent columns in the observed multicolored transverse arrays did not change as $\theta_p$ varied.

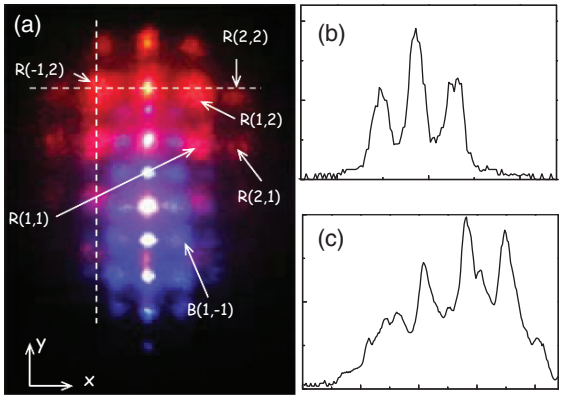


**Fig. 8.2.** The picture of the experimentally observed two-dimensional multicolored transverse arrays (**a**), and the corresponding intensity spectra of a row of multicolored transverse patterns crossing $R(1, 2)$ (**b**) and a column of multicolored transverse patterns crossing $R(-1, 2)$ (**c**) as labeled with *dashed line* in (**a**)

In the presence of the off-axis $\overrightarrow{k_2}$ beam, the spatial breakup of the elliptic input $\overrightarrow{k_1}$ beam was enhanced, as evidenced by the distinct columns in the two-dimensional multicolored transverse arrays. The enhanced spatial beam breakup was a direct result of energy transfer involved in the cascaded non-collinearly quadratic processes among different two-dimensional patterns. Fundamentally different from the two-dimensional discrete solitons in optically induced nonlinear lattices [18] or multiple filaments in air [6, 19], the approach demonstrated here can not only be served as a novel mechanism for the two-dimensional array generation with pump intensities below the material damage thresholds, but also provide us more degrees of freedom to control two-dimensional arrays of quadratic spatial solitons. This may stimulate further experiments to explore the fundamental dynamics of wave-packet breakup or collapse during wave propagation in quadratic nonlinear media, and may bring about various novel applications.

## 8.3 Transient Grating Probing

As the generation of two-dimensional multicolored transverse arrays was based on the cascaded non-collinearly quadratic couplings, the effective refractive index of the nonlinear crystal was modulated correspondingly. This established two-dimensional transient gratings. Experimentally, such two-dimensional transient gratings could be imaged and probed with synchronous coherent beams. In order to show this point clearly, as shown in Fig. 8.3a, a super-continuum pulse was produced by focusing another off-axis beam $\overrightarrow{k_3}$ (split from $\overrightarrow{k_2}$) into a 2 mm-thick sapphire plate. The residual FW pump pulses at 800 nm in the super-continuum were removed after passing through a short-pass filter with a cutoff wavelength around 750 nm. Here, the $\overrightarrow{k_3}$ beam is collimated down to the 4 mm thick BBO crystal and crossly overlapped with the $\overrightarrow{k_1}$ and $\overrightarrow{k_2}$ beams. As presented in Fig. 8.3b, the synchronously seeded super-continuum pulses were at first diffracted by the transient gratings and then amplified at the diffracted directions, leading to the generation of two-dimensional multicolored up-converted parametric amplifications.

Figure 8.3c presents the experimentally observed multicolored up-converted parametric amplifications as the super-continuum was seeded at $R(1, 2)$. The corresponding spectra of some selected spots were plotted in Fig. 8.3d. In order to identify the up-converted patterns from above multicolored transverse arrays, we labeled different spots in the two-dimensional multicolored up-converted parametric amplifications by $\mathrm{G}(n, m)$ with the seeded super-continuum beam as $G(0, 0)$. As the generated two-dimensional transient gratings were probed by the super-continuum beam at different positions with various geometric angles, the super-continuum beam would be diffracted and then amplified in different ways. These led to tunable multicolored up-converted parametric amplifications within different ranges. Figure 8.4 gives

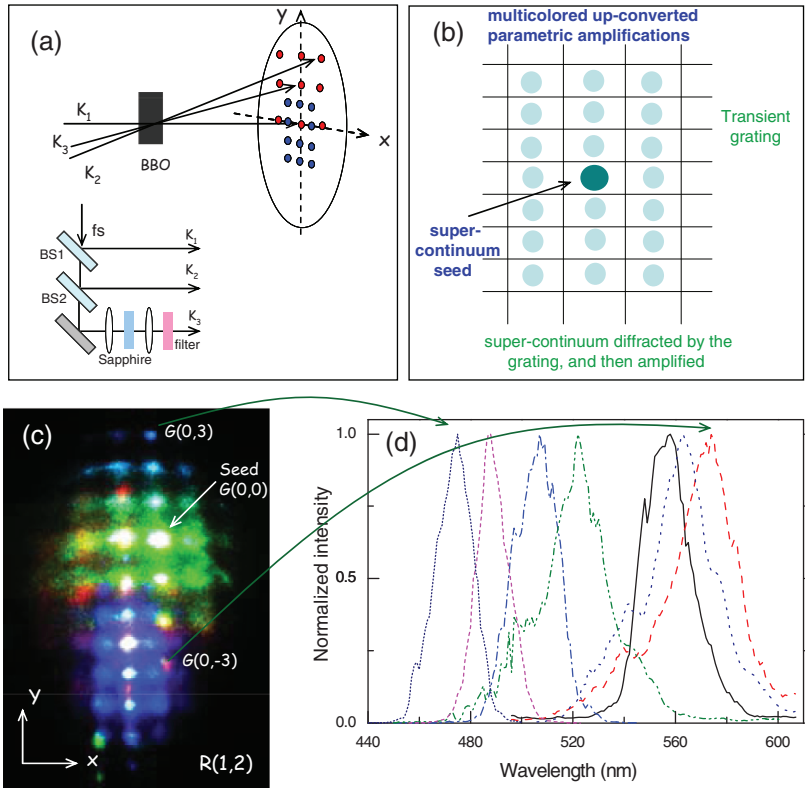


**Fig. 8.3.** (**a**) Experimental schematic for observation of multicolored up-converted parametric amplifications, where a super-continuum beam $k_3$ is used as a probe. (**b**) Diffraction and amplification of the seeded super-continuum pulse by the cascaded non-collinearly quadratic processes induced two-dimensional transient grating, which produces two-dimensional multicolored up-converted parametric amplifications. (**c**) Picture of the observed multicolored up-converted parametric amplification patterns as the super-continuum was seeded at $R(1,2)$. (**d**) Spectra of some selected spots $G(0,m)$ from multicolored up-converted parametric amplifications as shown in (**c**), where $m = 3,\ 2,\ 1,\ 0,\ -1,\ -2$, and $-3$, respectively, from left to right. BS: beam splitter

typical examples of two-dimensional multicolored up-converted parametric amplification patterns at different super-continuum seeding angles, where (a) and (b) correspond to the situations with super-continuum beams seeded at $R(2,1)$, and in the middle of $R(1,1)$, $R(1,2)$, $R(2,1)$, and $R(2,2)$, respectively. Figure 8.4c presents the spectra of some selected spots from the observed multicolored up-converted parametric amplifications as shown in Fig. 8.4b. The probe beam was not necessarily seeded at one of the spots of the two-dimensional multicolored transverse arrays for the observation of two-dimensional multicolored up-converted parametric amplifications since

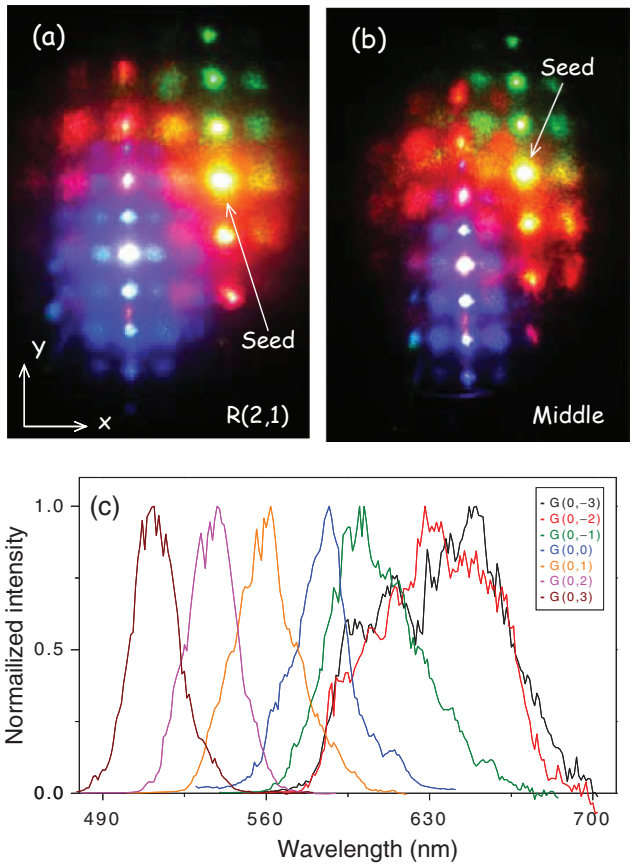


**Fig. 8.4.** Pictures of two-dimensional multicolored up-converted parametric amplifications observed with super-continuum seeded at (**a**) $R(2,1)$ and (**b**) in the middle of $R(1,1)$, $R(1,2)$, $R(2,1)$, and $R(2,2)$, respectively. (**c**) The spectra of some selected spots of multicolored up-converted parametric amplifications as shown in (**b**)

the formed gratings existed in the whole interaction region, and the resulted multicolored up-converted parametric amplification patterns covered almost the whole optical spectrum in the visible region.

The dependence of two-dimensional multicolored up-converted parametric amplifications on the cascaded non-collinearly quadratic processes induced transient gratings could be tested by changing the relative delays among $\overrightarrow{k_1}$, $\overrightarrow{k_2}$ and $\overrightarrow{k_3}$. For example, Fig. 8.5 presents the dependence of multicolored up-converted parametric amplification pattern upon the delays of $\overrightarrow{k_1}$ and $\overrightarrow{k_2}$ while keeping the delay of $\overrightarrow{k_3}$ unchanged. Obviously, the two-dimensional multicolored up-converted parametric amplification patterns shrank dramatically as the delays of $\overrightarrow{k_1}$ and $\overrightarrow{k_2}$ walked away, which caused the degeneration of

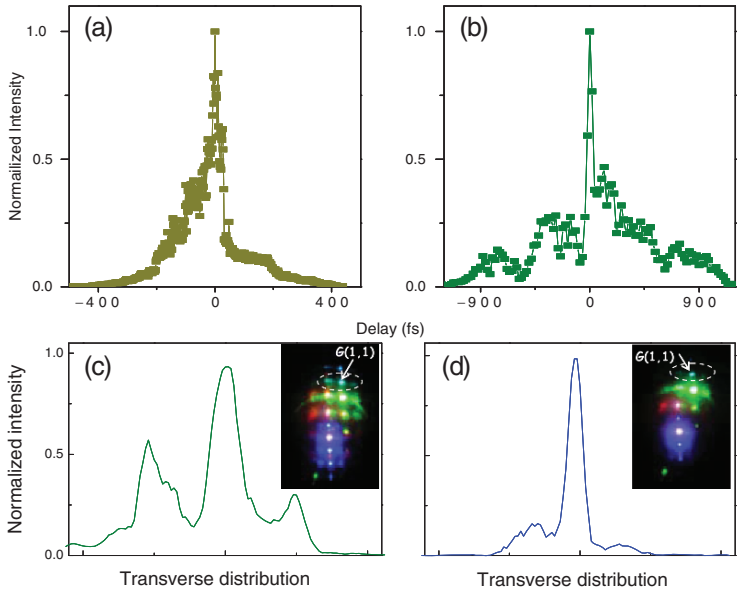


**Fig. 8.5.** Intensity dependences of multicolored up-converted parametric amplification patterns upon the delays of (**a**) $k_1$ and (**b**) $k_2$, respectively. Here, the $k_3$ is seeded at $R(1,2)$ and the up-converted pattern is selected to be $G(1,1)$ as labeled in the figures. (**c**) and (**d**) present the intensity spectra of a row of multicolored up-converted parametric amplification patterns crossing $G(0,1)$ as the delay of $k_2$ is changed to be 100 and 1,000 fs, respectively, while keeping $k_1$ and $k_3$ unchanged. The correspondingly observed pictures are also presented as the insets

the formed two-dimensional transient gratings. Furthermore, in the absence of transient gratings by blocking beam $\overrightarrow{k_2}$, the observed two-dimensional multicolored up-converted parametric amplifications degraded into a simple parametric amplification with patterns similar to that from beam $\overrightarrow{k_1}$. It clearly demonstrates that the multicolored up-converted parametric amplifications was produced by diffracting and amplifying seeded super-continuum pulse with the quadratic nonlinearities induced transient gratings.

Moreover, spectral coherence would be expected if the phase was preserved in the nonlinear amplifications along different directions, since they were from the same super-continuum pulse. We measured phase difference between two selected spots by using a so-called spectral interferometry technique. Figure 8.6a shows the setup for spectral interference technique. The beating signal on the charged coupled device could be written as

$$\begin{aligned} S(\omega) &= \left|E_1(\omega)\mathrm{e}^{\mathrm{i}\phi_1(\omega)} + E_2(\omega)\mathrm{e}^{\mathrm{i}[\phi_2(\omega)+\omega\tau]}\right|^2 \\ &= |E_1|^2 + |E_2|^2 + 2E_1E_2\cos(\omega\tau + \Delta\phi), \end{aligned} \tag{8.1}$$

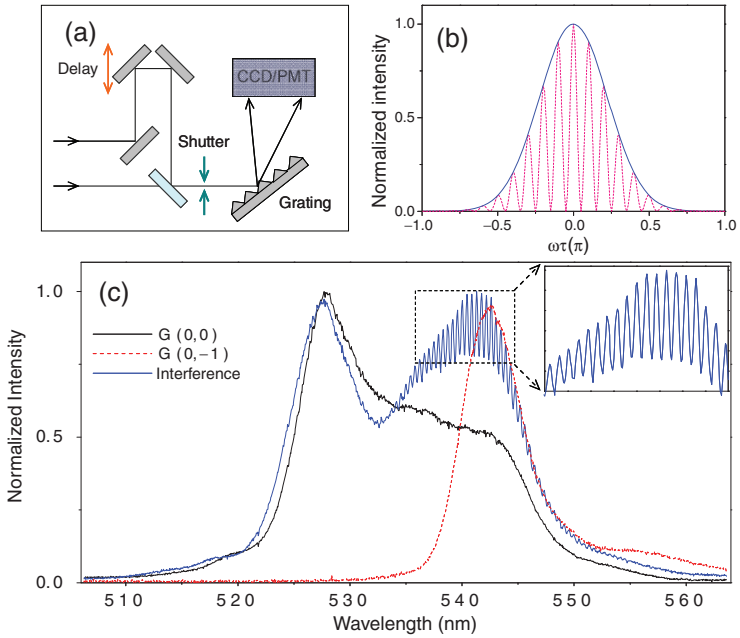


**Fig. 8.6.** (**a**) Experimental setup for spectral interference. (**b**) Simulated spectral interference patterns for pulses with constant (*dashed line*) and random (*solid line*) phase differences from shot to shot. (**c**) The measured spectral interference between two selected multicolored up-converted parametric amplification patterns with a preset delay and comparable intensities. CCD: charge coupled device; PMT: photomultiplier tube

where $\Delta\phi = \phi_2 - \phi_1$ is the phase difference between two interfering pulses of central frequency $\omega$ and preset delay of $\tau$. As shown in Fig. 8.6b, a stable interference pattern can be observed if the beating pulses have a constant phase difference, otherwise the interference patterns will smear out after several laser shots if the phase difference between the beating pulses varies randomly from shot to shot. Experimentally, as shown in Fig. 8.6c, reproducible spectral interference pattern after an average of several thousand laser shots were observed between two selected spots with a preset delay and relatively comparable intensities. Obviously, phase coherence was preserved during the diffraction and amplification of the probe pulse at different directions, which led to a constant phase difference between the amplified up-converted patterns at different colors.

Under the pump of FW pulses at 800 nm, multiple frequency up-conversions with different colors distributed in two-dimensional transverse patterns were demonstrated as a direct result of crossly coupled cascaded non-collinearly quadratic and multiple parametric processes, which exhibited features quite different from the standard optical parametric amplifications. As the probing super-continuum pulses include different spatiotemporal chirps in different

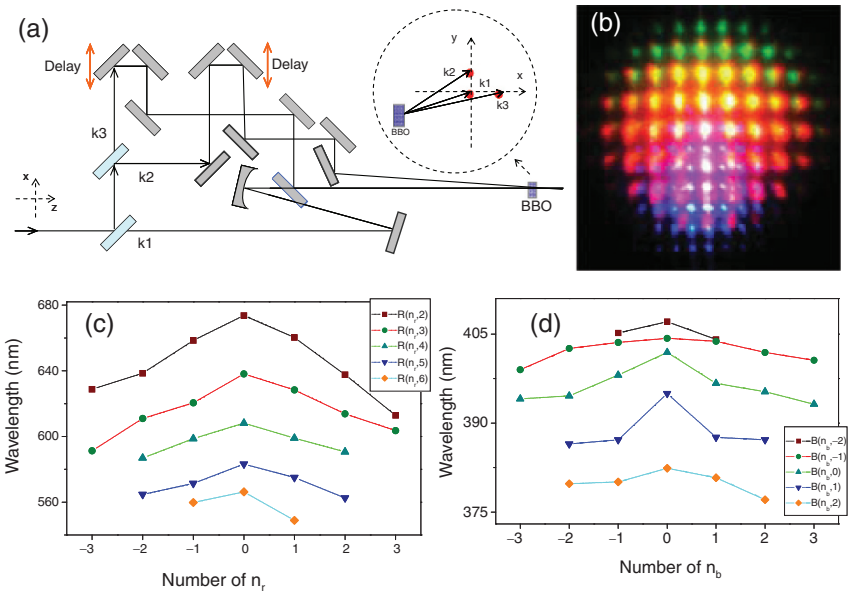


**Fig. 8.7.** (**a**) Experimental setup for observation of enhanced two-dimensional multicolored transverse arrays with a weak FW pulse $k_3$ split directly from FW pump pulse as the probe. (**b**) Picture of the observed enhanced two-dimensional multicolored transverse arrays. (**c**) and (**d**) plot the measured spectra of some selected spots as shown in (**b**)

spectral regions, the spatiotemporal dynamics of the involved cascaded non-collinearly quadratic processes could be investigated and the spatial distribution of the transient grating in the quadratic nonlinear medium could be dynamically imaged.

The transient gratings could be also observed by using a probing pulse directly split from the FW pulse. As shown in Fig. 8.7a, the $\overrightarrow{k_1}$, $\overrightarrow{k_2}$, and $\overrightarrow{k_3}$ beams were split directly from the FW pulses at 800 nm, and $\overrightarrow{k_3}$ pulse was very weak. Due to diffraction and amplification of the two-dimensional transient grating formed by $\overrightarrow{k_1}$ and $\overrightarrow{k_2}$, an significantly enhanced two-dimensional multicolored transverse arrays was observed as shown in Fig. 8.7b. More than 180 spots at different colors were actually produced by this novel technique, which could not be seen clearly in the picture due to the limitations of our digital camera. Differing from the observation of multicolored up-converted parametric amplifications with super-continuum pulse, here we synchronized $\overrightarrow{k_3}$ with $\overrightarrow{k_1}$ at the position where wave-packet breakup occurred, which also participated in the cascaded non-collinearly quadratic processes directly as $\overrightarrow{k_1}$ and $\overrightarrow{k_2}$ did. The wavelengths of different spots were measured. As shown in Fig. 8.7c, d, the measured central wavelengths of the adjacent spots agree

well with the required phase-matching conditions of the corresponding cascaded non-collinearly quadratic processes. The emitting red spots cover a quite broad band spectral range from 550 to 800 nm. The spots farther away from the center occupy shorter wavelengths due to the cascaded non-collinearly quadratic processes. The observation of such enhanced multicolored transverse arrays further indicates that spatial wave-packet breakup and the followed cascaded non-collinearly quadratic processes play crucial roles in forming of our two-dimensional arrays. The phase coherence between different spots form the enhanced two-dimensional arrays was tested by using the spectral interferometry technique in the frequency domain. With a proper preset delay, a clear spectral interference pattern between the selected patterns was observed after an average of several thousand laser shots, which indicated the two-dimensional patterns were actually multicolored coherent optical sources.

The coherent two-dimensional patterns could be further combined into one beam by using a hollow fiber with a scheme as shown in Fig. 8.8a. In the experiment, all the spots from the enhanced two-dimensional multicolored transverse arrays were focused into a $L = 50\,\text{mm}$, $D = 1.0\,\text{mm}$ hollow fiber with a $f = 60$-mm achromatic lens. As shown in Fig. 8.8b, except the blue part around 400 nm, a quite broadband spectrum (590–820 nm) could be obtained at the end of the hollow fiber. The contributions from the outer spots with wavelengths shorter than 590 nm were almost eliminated due to their

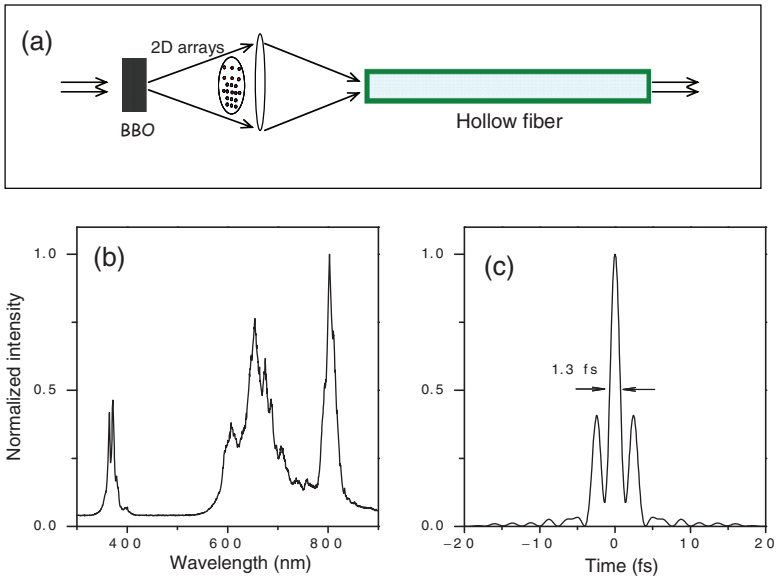


**Fig. 8.8.** (**a**) Experimental schematic for two-dimensional patterns combination using a hollow fiber. (**b**) The spectrum of the combined beam after a 50-mm hollow fiber, and (**c**) the corresponding transform-limited pulse by assuming the spectrum is chirped free with wavelength longer than 590 nm

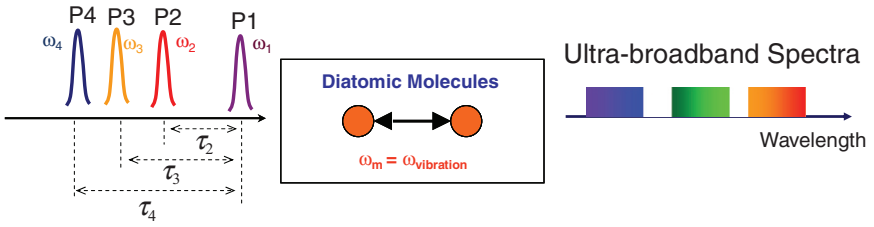


**Fig. 8.9.** Schematic for multicolored impulsive stimulated Raman scatterings to obtain ultra-broadband spectra with pump pulses at different frequencies selected from our two-dimensional arrays

relative weak intensities as compared with the inner spots and the waveguide effects of the hollow fiber. By using specially designed double chirped mirror pairs [20] or spatial light modulators [21] for dispersion compensation, the broadband spectrum can be compressed to produce ultrashort pulse. As shown in Fig. 8.8c, it can result in a transform-limited pulse in sub-5 fs range. Significantly, the combined beam has a high pulse energy (∼44 μJ). The generation of high-peak-power optical pulse with duration down to sub-5 fs range is particularly important for a number of fundamental experiments, such as single attosecond pulse generation by high-order harmonic generation [22], ultrafast nonlinear spectroscopy, strong-field light-matter interactions, and various nonlinear processes.

Moreover, the coherent two-dimensional multicolored arrays could also be used as pumps for multicolored impulsive stimulated Raman scatterings [23]. As shown in Fig. 8.9, we could select one spot from the coherent two-dimensional arrays at frequency $\omega_1$ with pulse duration shorter than the period of the Raman-active vibrational mode as the first pump beam, which leaved the molecules in a vibrational state. The modulated refractive index could be probed by the delayed coherent pulses at different frequencies ($\omega_2$, $\omega_3$, $\omega_4$ ...) selected from the two-dimensional arrays. It was expected that each pulse itself would lead to a coherent broadened spectrum with central wavelength as the probe. Then, an ultra-broadband spectrum could be obtained to produce sub-fs pulses [24] when they were adjusted to walk together temporarily.

## 8.4 Weak Beam Control of Two-Dimensional Arrays

The strong nonlinear couplings between FW and SH fields are responsible for the collapses of optical waves during second harmonic generation processes in quadratic media [15–17]. It was demonstrated that one-dimensional multiple quadratic spatial solitons could be controlled by seeding a weak SH beam at the input of the nonlinear medium [8]. Since our two-dimensional arrays were formed on the basis of the generation of one-dimensional multiple

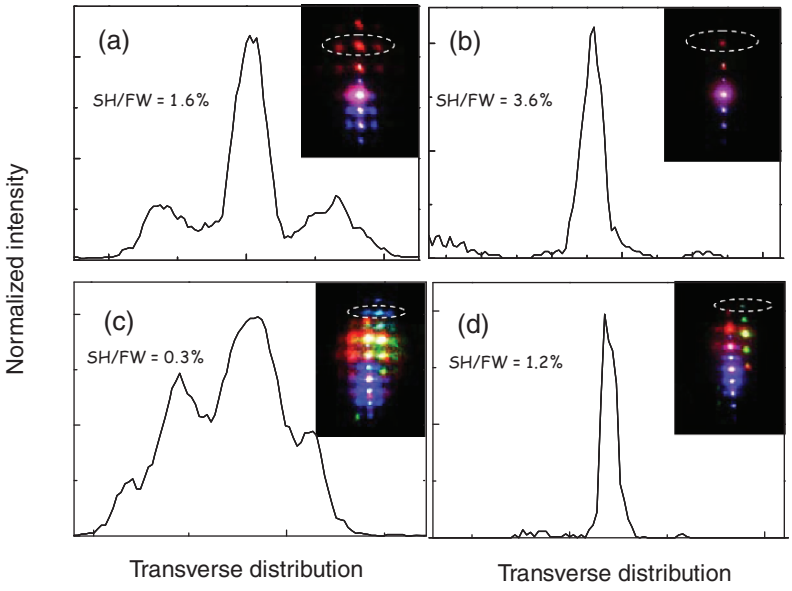


**Fig. 8.10.** Intensity spectra of a row of multicolored transverse patterns crossing $R(0,2)$ (**a, b**) and a row of multicolored up-converted parametric amplification patterns crossing $G(0,2)$ (**c, d**) under different pulse energy ratios SH/FW. The experimentally observed pictures are also presented as insets

quadratic spatial solitons, it is straightforward to expect that the observed two-dimensional arrays can also be controlled by a weak SH beam.

Figure 8.10a, b present the dependent results of two-dimensional multicolored transverse arrays on the SH control beam. The two-dimensional patterns were switched to one-dimensional ones as the energy ratio SH/FW reached 3.6%. In order to demonstrate the dependence of the control on the relative phase shift between the FW pump and weak SH control pulses, a 1-mm-thick $CaF_2$ plate was inserted between two BBO crystals to introduce a tunable relative phase shift. By tilting the $CaF_2$ plate, the relative phase shift could be varied from 0 to $2\pi$ readily. The experimental results showed that the control of two-dimensional multicolored transverse arrays was independent on the relative phase between the $\overrightarrow{k_1}$ FW and SH control pulses, which was consistent with the phase-insensitive control of one-dimensional multiple quadratic spatial solitons [8] caused by the spatial collapse of the spatially elliptic input beam. Obviously, the weak SH control beam brought about the same suppression of the two-dimensional patterns as it did on the one-dimensional multiple quadratic spatial solitons induced by the elliptic beam. This further suggests that the spatial collapse of the on-axis $\overrightarrow{k_1}$ beam is responsible for the formation of our two-dimensional multicolored transverse arrays by means of cascaded non-collinearly quadratic processes.

Figure 8.10c, d present the dependence of multicolored up-converted parametric amplifications with super-continuum seeding at $R(1,2)$ under different SH/FW ratios, demonstrating that the two-dimensional multicolored up-converted parametric amplifications could also be controlled by weak SH seeding pulses. Two-dimensional multicolored up-converted parametric amplification patterns were switched into one-dimensional ones when ratio SH/FW was about 1.2%. The threshold energy ratio SH/FW to suppress the two-dimensional multicolored up-converted parametric amplification patterns was consistent with those to suppress one-dimensional multiple quadratic spatial solitons [8] and two-dimensional multicolored transverse arrays.

Similar to one-dimensional multiple quadratic spatial solitons and two-dimensional multicolored transverse arrays, the control of two-dimensional multicolored up-converted parametric amplifications also exhibited a phase-independent feature. This implies that multiple coherent strong pulses could be controlled by using a weak SH beam without any predetermined phase relative to the pulses to be controlled, which may support a novel kind of phase-insensitive all-optical control with a weak beam to control multiple strong beams. As multicolored up-conversions in two-dimensional multicolored up-converted parametric amplifications could be coherent synthesized, a weak SH control of the two-dimensional multicolored up-converted parametric amplifications could facilitate an all-optical control of the relative intensities of different multicolored up-converted parametric amplification patterns, and consequently support an all-optical control of coherent pulses synthesis. This may find interesting applications in all-optical quantum coherent control.

## 8.5 Colored Conical Emissions

As shown in Fig. 8.11a, spatiotemporal modulational instabilities occur as a result of exponential growth of perturbations during propagations of wavepackets in nonlinear media as both dispersion and diffraction are present [1,2,13]. Assisted by spatiotemporal modulational instabilities, colored conical emissions by means of second harmonic generation involves multiple three-photon processes, which can be described by an intuitionistic picture as shown in Fig. 8.11b [2, 13]. Under the pump of on-axis pulses at the FW frequency $\omega$, spatiotemporal modulation instabilities induce decay of SH photons $2\omega$ into photon pairs at frequencies $\omega_{\pm} = \omega \pm \delta$ traveling with opposite off-axis angles, resulting in colored conical emissions. Colored conical emissions could be clearly observed under a high-intensity pump, and it is intrinsically originated from exponential growth of noises or perturbations as a result of spatiotemporal modulational instability. The maximum nonlinear growth occurs at phase-matched directions for different wavelengths, with a characteristic of phase-matched parametric decay of the SH pulses. Accordingly, distinct colored conical emissions appear as the FW pump pulses are aligned at the second harmonic generation phase-matching condition. It is not necessary to

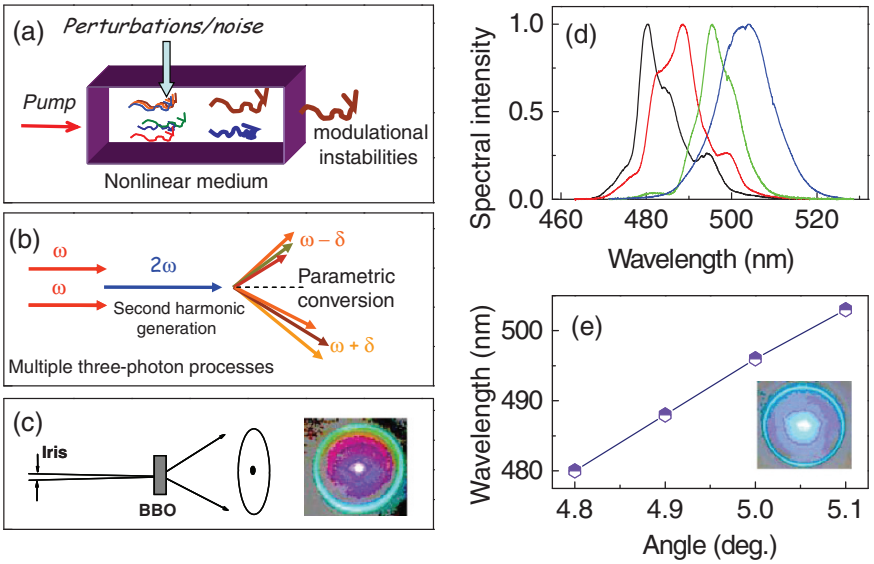


**Fig. 8.11.** (**a**) Exponential growth of perturbations during propagations of wavepackets in nonlinear media lead to the occurrences of modulational instabilities. (**b**) Multiple three-photon processes and (**c**) experimental schematic for observation of colored conical emissions during second harmonic generation in a thick quadratic nonlinear medium. (**d**) The spectra of the blue-green conical emission recorded with a small angular window. (**e**) The corresponding central wavelengths of the spectra as shown in (**d**) as a function of emission angles. The insets of (**c**) and (**e**) show the typical pictures of colored conical emissions as the FW pump pulses passing through a smaller iris (**c**), and at the optimum pumping chirp and angular spectra (**e**), respectively

have an input spatial asymmetry for the input beam as required for the generation of two-dimensional multicolored transverse arrays and multicolored up-converted parametric amplifications as discussed above [12].

In our experiments, as shown in Fig. 8.11c, the fs pulses from the amplified Ti:sapphire system with energy of 650 μJ/pulse were directly focused into a 6-mm-thick BBO crystal (type I, 29.18° cut) by using a lens with a focusing length of 1,000 mm. As shown in Fig. 8.11e, a bright blue-green cone with a conical angle of $\sim$ 5.0° emerged around the propagation axis when the pump reached a sufficiently high intensity and the BBO crystal was rotated to maximize the second harmonic generation. As plotted in Fig. 8.11d, e, the blue-green conical emission peaked near 500 nm and exhibited an angular width of about 0.4° (4.77°–5.17°). Spatiotemporal modulational instabilities and thus the induced colored conical emissions changed when the chirp (time) or beam divergence (space) of the FW pump pulse was varied. We used an iris placed before the concave mirror to vary the diameter and divergence of the laser beam focused into the BBO crystal. As presented in Fig. 8.11c, when

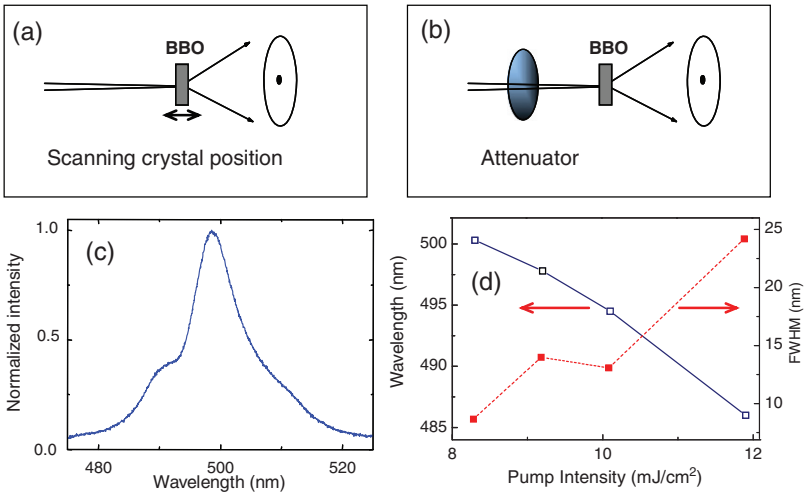


**Fig. 8.12.** Experimental schemes for change of pump intensities by (**a**) scanning the crystal along the focusing direction and (**b**) rotating a tunable attenuator before the BBO crystal. (**c**) The typical spectral profiles of blue-green conical emission. (**d**) The central wavelengths and FWHMs of the spectra of blue-green conical emission as a function of pump intensity

the iris was changed to a smaller diameter, the blue-green conical emission became less intense, and a red semiconical emission appeared inside the blue-green conical emission. On the other hand, red semiconical emissions could also be observed within the weakened blue-green conical emission as small negative chirps were intentionally introduced to the FW pump pulses. These observations clearly suggest that space and time degrees of freedom played the same role to entail colored conical emissions.

The pump intensity dependent spectral profile is one of the most important features of modulational instabilities [2, 3, 25]. As shown in Fig. 8.12a, b, the pump intensity on the facet of BBO crystal was changed by either scanning the position of the crystal along the focusing direction or rotating a tunable attenuator before the BBO crystal. The spectral features of the blue-green conical emission under different pump intensities are also plotted in Fig. 8.12. As the pump intensity increased, blue-shifted spectra were observed with increased full width at half maximum (FWHM). This implied strong nonlinear couplings among the involved multiple three-photon processes.

## 8.6 Seeded Amplification of Colored Conical Emission

Seeded amplification of colored conical emission could be realized by seeding with an accurately synchronized super-continuum pulse [14]. The injected seed could attain exponential gain along a certain conical angle of colored

conical emissions and the nonlinear gain was assisted by spatiotemporal modulational instabilities, leading to a FW pump intensity dependence of the parametric gain. Intrinsically different from standard optical parametric amplification, seeded amplification of colored conical emission is pumped by the FW pulses, and up-converted amplification occurs as a direct result of multiple quadratic processes (second harmonic generation and parametric amplification). Rather than a simple combination, second harmonic generation and parametric amplifications are coupled each other. Nonlinear phase shifts induced by phase-matched second harmonic generation entail seeded amplification of colored conical emission output spectra dependent on the FW pump intensity. Strong couplings between FW and SH pulses may further balance the group velocity mismatching and dispersion, enabling large interaction length to output a quite high pulse energy of up-converted amplification. From the practical points of view, seeded amplification of colored conical emission supports a broadband fs up-conversion with a quite simple setup.

In the experiments, as shown in Fig. 8.13a, a weak FW pulse split from the output of the laser system was attenuated and then focused into a 2 mm thick sapphire plate to generate a super-continuum beam, which was further collimated to the BBO crystal as the seed pulses. The residual FW pulses were used to generate colored conical emissions with a scheme as discussed above. As shown in Fig. 8.13a, a sparkling green point appeared at point A just as a pearl over the blue-green conical emission ring. The seeded amplification of colored conical emission output beam showed a beam divergence about 0.7 mrad, and the corresponding $M^2$ parameter was measured to be 5.4 at a typical operation with the output pulse energy of 100 μJ under the fundamental pump intensity of 12 mJ cm$^{-2}$. The maximum seeded amplification of colored conical emission output pulse energy reached up to ∼150 μJ as the FW pump pulse energy was increased to 650 μJ (∼14 mJ cm$^{-2}$). This was at least one order of magnitude higher than those obtained with comparable FW pump pulses by using the standard non-collinear optical parametric amplification scheme.

Figure 8.13b, c presents the typical spectrum of seeded amplification of colored conical emission at a pump intensity of 10.6 mJ cm$^{-2}$, and the corresponding central wavelengths and FWHMs of the spectra versus the FW pump intensity, respectively. Seeded amplification of blue-green conical emission produced output pulses centered around 500 nm with FWHMs typically larger than 20 nm. Interestingly, seeded amplification of colored conical emission exhibited blue-shifted frequencies of amplification at higher FW pump intensities, implying that the corresponding photon-momentum conservation was modulated, which is actually one of the key features of seeded amplification of colored conical emission that differs from the standard optical parametric amplification. This can be qualitatively understood as follows. Since seeded amplification of colored conical emission consisted of multiple quadratic processes, FW and SH pulses in the second harmonic generation process strongly coupled with the signal and idler pulses in the parametric process. Interplay of

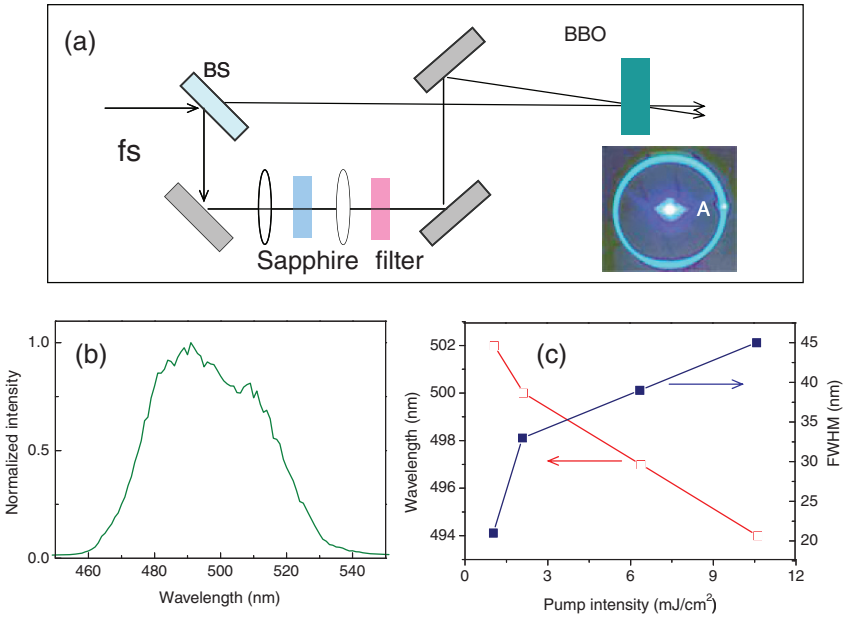


**Fig. 8.13.** (**a**) Experimental setup for seeded amplification of colored conical emission. (**b**) The typical spectrum of seeded amplification of colored conical emission at a pump intensity of 10.6 mJ $cm^{-2}$, and (**c**) the corresponding central wavelengths and FWHMs of the spectra of seeded amplification of colored conical emission on the ring as a function of pump intensity. The inset in (**a**) is the picture of the observed seeded amplification of colored conical emission as the seed angle is set to be 5°. BS: beam split

such multiple nonlinear processes caused nonlinear phase shifts to the pump pulses and modulated the effective nonlinear refractive index of the crystal. Consequently, the phase-matching condition and thus the photon-momentum conservation in seeded amplification of colored conical emission changed under different pump intensities. Therefore, for a given crossing angle and delay between the FW pump and super-continuum seed pulses, different spectral profiles could be observed as the FW pump intensities increase.

As colored conical emissions showed different spectra at different conical angles, seeded amplification of colored conical emission with different wavelengths could be obtained by varying the seed angle of the super-continuum beam. Figure 8.14 shows some typical pictures of seeded amplification of colored conical emission observed under different seeding angles. The detailed wavelength dependence of seeded amplification of colored conical emission on the seed angle is plotted in the right of Fig. 8.14, which shows a tunable range from 500 to 798 nm as the seed angle is varied from 5° to 0.68°. As a result of the self-phase-modulation processes in the sapphire plate, there existed a spectral chirp in the seeded super-continuum pulse. Therefore, the

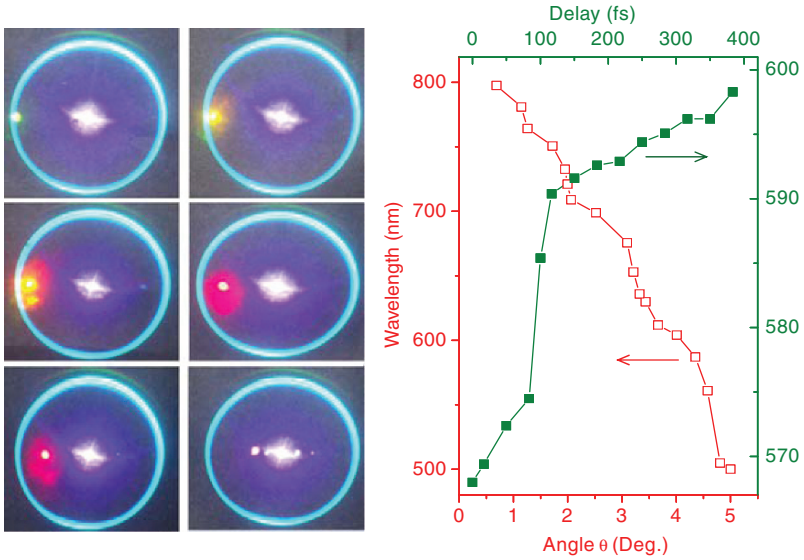


**Fig. 8.14.** Pictures of observed seeded amplification of colored conical emissions with super-continuum seeded at various angles (*left*). The dependences of the central wavelengths of seeded amplification of colored conical emissions as the seed angle and the delay between the FW and the super-continuum pulses are adjusted (*right*)

wavelength of seeded amplification of colored conical emission could also be tuned by adjusting the delay between FW pump and super-continuum seed pulses. The delay dependent tunable results are also presented in Fig. 8.14 as the seed angle was set as 4.5°. Obviously, tunable ultrashort pulses can be generated based on seeded amplification of colored conical emission, which supports significant amplification of up-converted pulses under infrared pump.

Carrier envelope phase stabilized fs pulses could be obtained by different frequency generation between the seeded amplification of colored conical emission and the FW pump pulses [26]. With a seed from self-phase-modulation broadened replica of a FW pump pulse and phase preservation in the amplification process, the amplified signal differs from FW pump pulse in carrier envelope phase by a constant value of $\pi/2$. Therefore, as shown in Fig. 8.15, the generated signal pulses by different frequency generation show a constant carrier envelope phase. In the experiments, we used a 1 kHz Ti:Sapphire regenerative amplifier to produce 1.4 mJ pulses of 40 fs duration at 800 nm. As shown in Fig. 8.15a, a part of output fs pulse with energy of 690 μJ was used to generate seeded amplification of colored conical emission based on a scheme as shown in Fig. 8.13, and the residual FW pulse with energy of 710 μJ was used for different frequency generation process. The different frequency generation signal in infrared optical region generated in a 2 mm thick BBO crystal (type-I, 31.5° cut) could be further frequency doubled to the visible

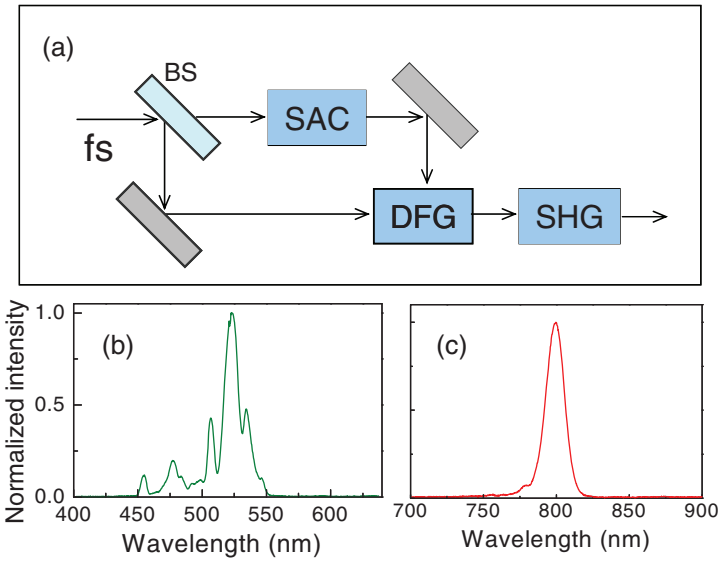


**Fig. 8.15.** (**a**) Experimental layout for generation of carrier envelope phase stabilized fs pulses by different frequency generation between the seeded amplification of colored conical emission and FW pump pulses. The spectral profiles of seeded amplification of colored conical emission and generated carrier envelope phase stabilized idler pulses are plotted in (**c**) and (**d**), respectively. BS: beam split; SAC: seeded amplification of colored conical emission; DFG: different frequency generation

region using another 2 mm thick BBO crystal (type-I, 19.8° cut). As shown in Fig. 8.15b, c, carrier envelope phase stabilized fs pulse centered at 800 nm could be generated after the second harmonic generation crystal as the central wavelength of the seeded amplification of colored conical emission pulse was tuned to 533 nm.

The carrier envelope phase stabilization of the generated different frequency generation pulse was verified by using a non-collinear optical parametric amplification based $f-2f$ spectral interference scheme [27,28]. As plotted in Fig. 8.16a, a stable interference pattern between the $f-2f$ beating pulses was observed, which indicated a stabilized carrier envelope phase of the different frequency generation signal pulse. The shot-to-shot drifts of the measured carrier envelope phase were calculated and plotted in Fig. 8.16b for the carrier envelope phase stabilized signal pulses. The carrier envelope phase drifts of the pulses emitted directly from the laser system were also plotted in Fig. 8.16c for comparison, which changed randomly from shot to shot without stabilization.

Since seeded amplification of colored conical emission exhibits a widely tunable range, the carrier envelope phase stabilized different frequency generation pulses can be tuned accordingly. As the central wavelength of seeded amplification of colored conical emission was tuned from 500 to 798 nm, as shown in Fig. 8.16d, the carrier envelope phase stabilized different frequency

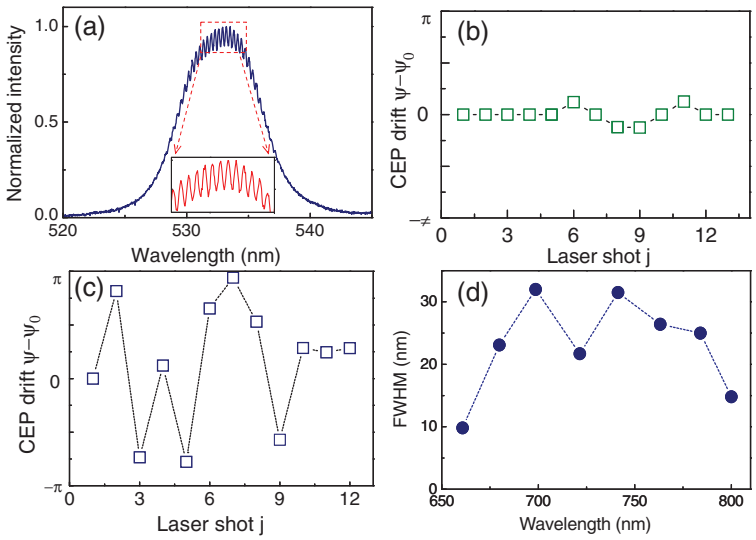


**Fig. 8.16.** (**a**) Spectral interference result of the generated carrier envelope phase stabilized pulses. (**b**) and (**c**) are the shot-to-shot carrier envelope phase drifts of the carrier envelope phase stabilized pulses and the pulses emitted directly from Ti:sapphire laser, respectively. (**d**) The measured FWHMs of the spectra of carrier envelope phase stabilized idler pulses as the central wavelength is tuned

generation pulses could be tuned from 660 to 800 nm with an FWHM of the spectrum varied between 10 and 32 nm, which correspond to a tunable range from 1,320 to 1,600 nm in the infrared region before the final second harmonic generation crystal.

## 8.7 Conclusions

As one of the most important and fascinating phenomena that have been observed so far in the propagation of intense laser pulses in nonlinear media, light wave collapse has attracted an ever-growing research interest, and has stimulated some interesting topics on fundamental physics and facilitated a variety of applications. Temporal, spatial, or spatiotemporal collapse of intense optical wave packets has been observed in various nonlinear systems. Nevertheless, the fundamental features of multidimensional wave-packet collapse have been left thus far widely unexplored due to the limit of material damage thresholds. We review here our experimental studies of two-dimensional multicolored solitary arrays with low pump intensities and colored conical emissions during second harmonic generation processes as a result of collapses of fs pulses in quadratic media, which showed various applications in different aspects. We summarize our main results as follows. (a) Two-dimensional multicolored transverse arrays were generated in a quadratic nonlinear medium

under the pump of two crossly overlapped fs beams. The experimental observation of two-dimensional patterns demonstrated the spatial breakup of the input elliptic beam and cascaded non-collinearly quadratic processes as a novel mechanism to form two-dimensional patterns at low pump intensities below the material damage threshold. (b) Multicolored up-conversion parametric amplification was realized as a super-continuum probe pulse was diffracted by the transient grating established in the cascaded non-collinearly quadratic processes and then, the diffracted super-continuum pulses attained nonlinear growths with phase preservation along different directions. This presents further evidence of cascaded non-collinearly quadratic processes that were responsible for the formation of two-dimensional patterns. The synchronized super-continuum pulses provided a direct imaging of the spatial distribution of the transient grating in the quadratic medium and thus, diffraction from the transient grating could be used to probe the dynamics of the cascaded non-collinearly quadratic processes. Multiple parametric amplifications concurred with frequency up-conversion, interplay of cascaded non-collinearly quadratic and multiple parametric processes brought about unique features different from standard optical parametric amplification. (c) The two-dimensional arrays could be suppressed through weak beam control of the induced quadratic spatial solitary waves. This provides further evidence that two-dimensional patterns were originated from the spatial beam breakup of the elliptic pump and the induced quadratic spatial solitons equivalently functioned as new beams in the cascaded nonlinear couplings. (d) Colored conical emissions could be observed as a result of spatiotemporal collapse of fs pulses in a quadratic medium. Seeded amplification of colored conical emission was demonstrated to support ultra-broadband and tunable up-conversion, wherein interplay of multiple nonlinear processes makes seeded amplification of colored conical emission differ from standard optical parametric amplifications. Difference frequency generation between pump and seeded amplification of colored conical emission pulses was demonstrated to exhibit a constant carrier envelope phase, which can be used as a novel all-optical control of carrier envelope phase. The carrier envelope phase stabilization was verified and broadband tunable carrier envelope phase pulses were realized. Finally, we would like to point out that of ultrashort pulse collapses in quadratic media include abundant unrevealed features, further experimental and theoretical investigations are required to fully understand the ultrafast dynamics and fundamental physics related with ultrashort pulse propagation.

## Acknowledgements

This work was supported in part by National Natural Science Fund (Grants 10774045, 10525416 and 10804032), Projects from Shanghai Science and Technology Commission (Grants 06JC14025, 06SR07102 and 08ZR1407100), National Basic Research Program of China (Grant 2006CB806005), Key projects from Chinese Ministry of Education (Grant 108058), Program for

Changjiang Scholars and Innovative Research Team in University, and Shanghai Educational Development Foundation (Grant 2008CG29). Contributions from Heping Zeng's group members and students (Jingxin Ding, Kun Wu, E Wu, Han Xu, Xuan Yang, Hua Cai, and Yan Peng) are highly appreciated.

## References

1. C. Conti, S. Trillo, P.D. Trapani, G. Valiulis, A. Piskarskas, O. Jedrkiewicz, J. Trull, Nonlinear electromagnetic X waves. Phys. Rev. Lett. **90**, 170406 (2003)
2. S. Trillo, C. Conti, P.D. Trapani, O. Jedrkiewicz, J. Trull, G. Valiulis, G. Bellanca, Colored conical emission by means of second-harmonic generation. Opt. Lett. **27**, 1451 (2002)
3. R.A. Fuerst, D.M. Baboiu, B. Lawrence, W.E. Torruellas, G.I. Stegeman, Spatial modulational instability and multisolitonlike generation in a quadratically nonlinear optical medium. Phys. Rev. Lett. **78**, 2756 (1997)
4. S. Polyakov, R. Malendevich, L. Jankovic, G.I. Stegeman, C. Bosshard, P. Gunter, Effects of anisotropic diffraction on quadratic multisoliton excitation in noncritically phase-matched crystals. Opt. Lett. **27**, 1049 (2002)
5. H. Kim, L. Jankovic, G.I. Stegeman, S. Carrasco, L. Torner, D. Eger, M. Katz, Quadratic spatial solitons in periodically poled $KTiOPO_4$. Opt. Lett. **28**, 640 (2003)
6. A. Dubietis, G. Tamošauskas, G. Fibich, B. Ilan, Multiple filamentation induced by input-beam ellipticity. Opt. Lett. **29**, 1126 (2004)
7. S. Carrasco, S. Polyakov, H. Kim, L. Jankovic, G.I. Stegeman, Observation of multiple soliton generation mediated by amplification of asymmetries. Phys. Rev. E **67**, 046616 (2003)
8. S. Polyakov, H. Kim, L. Jankovic, G.I. Stegeman, M. Katz, Weak beam control of multiple quadratic soliton generation. Opt. Lett. **28**, 1451 (2003)
9. G. Assanto, G. Stegeman, M. Sheik-Bahae, E. Van Stryland, All-optical switching devices based on large nonlinear phase shifts from second harmonic generation. Appl. Phys. Lett. **62**, 1323 (1993)
10. X. Liu, L. Qian, F. Wise, High-energy pulse compression by use of negative phase shif ts produced by the cascade $\chi^{(2)}$: $\chi^{(2)}$ nonlinearity. Opt. Lett. **24**, 1777 (1999)
11. L.J. Qian, X. Liu, F.W. Wise, Femtosecond Kerr-lens mode locking with negative nonlinear phase shifts. Opt. Lett. **24**, 166 (1999)
12. H. Zeng, J. Wu, H. Xu, K. Wu, Generation and weak beam control of two-dimensional multicolored arrays in a quadratic nonlinear medium. Phys. Rev. Lett. **96**, 083902 (2006)
13. H. Zeng, J. Wu, H. Xu, K. Wu, E. Wu, colored conical emission by means of second harmonic generation in a quadratically nonlinear medium. Phys. Rev. Lett. **92**, 143903 (2004)
14. H. Zeng, K. Wu, H. Xu, J. Wu, Seeded amplification of colored conical emission via spatiotemporal modulational instability. Appl. Phys. Lett. **87**, 061102 (2005)
15. M. Segev, G.I. Stegeman, Self-trapping of optical beams: spatial solitons. Phys. Today **51**, 42 (1998)
16. A.V. Buryak, Y.S. Kivshar, Spatial optical solitons governed by quadratic nonlinearity. Opt. Lett. **19**, 1612 (1994)

17. K.D. Moll, A.L. Gaeta, Mutual spatio-temporal collapse of femtosecond pulses, quantum electronics and laser science conference, Long Beach (California), USA (2002)
18. J.W. Fleischer, M. Segev, N.K. Efremidis, D.N. Christodoulides, Observation of two-dimensional discrete solitons in optically induced nonlinear photonic lattices. Nature (London) **422**, 147 (2003)
19. G. Méchain, A. Couairon, M. Franco, B. Prade, A. Mysyrowicz, Organizing multiple femtosecond filaments in air. Phys. Rev. Lett. **93**, 035003 (2004)
20. E.J. Mayer, J. Mbius, A. Euteneuer, W.W. Rhle, R. Szipcs, Ultrabroadband chirped mirrors for femtosecond lasers. Opt. Lett. **22**, 528 (1997)
21. S. Guo, Z.Y. Rong, H.T. Wang, Y.R. Wang, L.Z. Cai, Phase-shifting with computer-generated holograms written on a spatial light modulator. Appl. Opt. **32**, 6514 (2003)
22. I.J. Sola, E. Mével, L. Elouga, E. Constant, V. Strelkov, L. Poletto, P. Villoresi, E. Benedetti, J.-P. Caumes, S. Stagira, C. Vozzi, G. Sansone, M. Nisoli, Controlling attosecond electron dynamics by phase-stabilized polarization gating. Nat. Phys. **2**, 319 (2006)
23. A. Nazarkin, G. Korn, Raman self-conversion of femtosecond laser pulses and generation of single-cycle radiation. Phys. Rev. A **58**, R61 (1998)
24. J. Wu and H. Zeng, Subfemtosecond pulse generation and multiplicative increase of pulse spacing in high-order stimulated Raman scattering. Opt. Lett. **28**, 1052 (2003)
25. K. Tai, A. Hasegawa, A. Tomita, Observation of modulational instability in optical fibers. Phys. Rev. Lett. **56**, 135 (1986)
26. K. Wu, X. Yang, H. Zeng, All-optical stabilization of carrier-envelope phase by use of difference frequency generation with seeded amplification of colored conical emission. Appl. Phys. B **88**, 189 (2007)
27. P. Baum, S. Lochbrunner, E. Riedle, Carrier-envelope phase fluctuations of amplified femtosecond pulses: characterization with a simple spatial interference setup. Appl. Phys. B **77**, 129 (2003)
28. K. Wu, Y. Peng, S. Xu, H. Zeng, All-optical control of the carrier-envelope phase with multi-stage optical parametric amplifiers verified with spectral interference. Appl. Phys. B **83**, 537 (2006)